TISSUE ENGINEERING
Volume 6, Number 5, 2000
Mary Ann Liebert, Inc.

Numerical Model and Experimental Validation of Microcarrier Motion in a Rotating Bioreactor

S.R. POLLACK, Ph.D.,[1] D.F. MEANEY Ph.D.,[1] E.M. LEVINE, Ph.D.,[2] M. LITT, D.Sc.,[1] and E.D. JOHNSTON, M.S.[1]

ABSTRACT

The equations of motion for microcarriers in a rotating bioreactor have been formulated and trajectories obtained using numerical techniques. An imaging system was built to validate the results by direct observation of microcarrier trajectories in the rotating frame of reference. The microcarrier motion observed by this imaging system was in excellent agreement with the numerical predictions of that motion. In the rotating frame of reference, microcarriers with density greater than the surrounding fluid medium followed a circular motion relative to the culture medium combined with a persistent migration and eventual collision with the outer wall of the reactor. However, for microcarrier density less the fluid medium, their circular motion migrated toward the central region of the reactor. When multiple microcarrier beads that are lighter than water are inserted into the reactor, the centrally directed migration results in the formation of clusters that are stabilized by tissue bridges formed by osteoblasts seeded onto the microcarriers. This system offers unique opportunities to monitor tissue synthesis on microcarriers using real-time optical techniques and to optimize the bioreactor operating conditions for exploiting this technology to study early bone tissue synthesis *in vitro*.

INTRODUCTION

A ROTATING BIOREACTOR known as a high aspect ratio vessel (HARV) was developed[1–3] in connection with the NASA program to study tissue and cellular engineering in a low-shear, nonturbulent, stimulated microgravity environment. This rotating bioreactor (Fig. 1) has a large radius-to-depth ratio providing a substantial surface area on the rear face for gas exchange through a gas-permeable membrane. To study cell and tissue cultivation in this bioreactor, microcarrier beads up to several hundred microns in diameter are co-injected with cells into the reactor through one of its ports and rotation is initiated at some desired angular velocity. Cells in this HARV vessel attach to the microcarriers and, under some circumstances, synthesize tissue bridges to form three-dimensional constructs. Previous analysis[4] proposed

[1]Department of Bioengineering University of Pennsylvania, Philadelphia, Pennsylvania.
[2]Wistar Institute, Philadelphia, Pennsylvania.
This work was presented at the Bioengineering Conference, June 16–20, 1999 Big Sky, Montana.

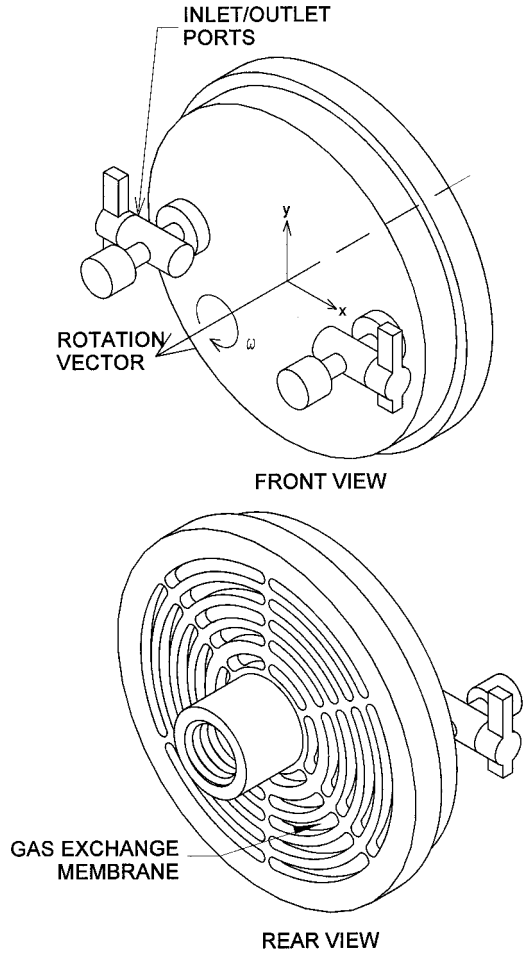

FIG. 1. Schematic of the rotating bioreactor (Synthecon Corporation, Houston, TX). This 55-mL disposable vessel has two inlet/outlet luer ports and rotates on its horizontal axis as shown. The gas exchange membrane allows passive exchange of gases to and from the media.

that the simultaneous gravitational, buoyant, centrifugal, coriolis, and drag forces combine to produce a "near static" condition for the small clusters of microcarriers with attached cells. The direction of the gravitational force changes cyclically in the rotating frame and, over one revolution of the reactor, the cells experience an average gravitational force of near zero, thereby leading to what has been described as the simulated microgravity environment.

It was the purpose of this effort to test this "near static" hypothesis with a rigorous mathematical analysis of this motion and to develop an experimental method to validate the trajectories and visualize microcarriers and cells in the reactor during rotation. We show that for microcarriers whose density is greater than the density of the culture medium, there is no near static position reached within the bioreactor but rather there are continuous collisions between the microcarriers and the walls of the bioreactor causing unquantified mechanical perturbations on tissue synthesis. In comparison, for microcarriers whose density is less than that of the medium, there is an aggregation of carriers with cells near the central axial region of the reactor that results in the formation of stable three-dimensional, porous scaffolds executing low-shear motion relative to the culture medium. As a result, the system provides an excellent simulated microgravity environment for tissue synthesis and study of microgravity effects on cell culture.

Some aspects of this problem were also considered by Gao *et al.*[5] They sought a closed-form solution to the governing equations of motion by using a Stokes flow approximation for the drag coefficient. In this

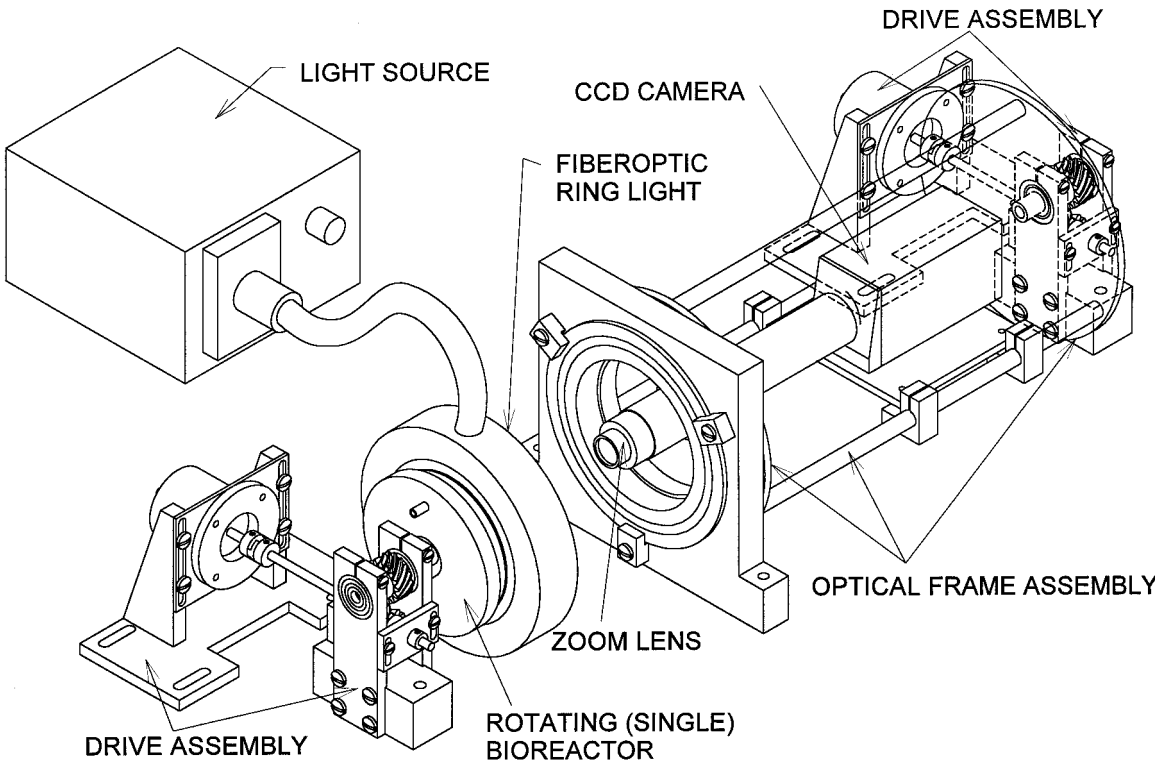

FIG. 2. Overview of the microcarrier imaging and particle tracking apparatus for the bioreactor. The camera rotates in synchrony with the bioreactor and uses a fiberoptics ringlight for illumination. Data can be stored on video tape or saved directly to memory.

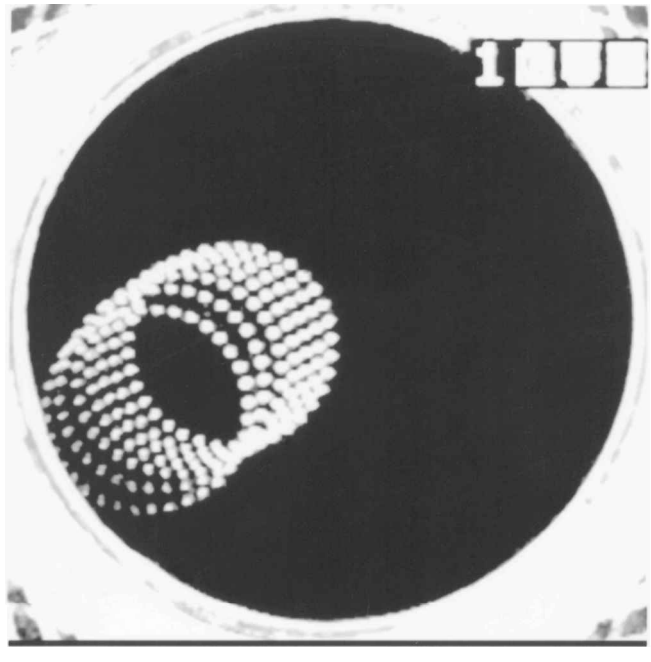

FIG. 3. Serial composite image of bead motion in rotating frame from center to outside wall. Polystyrene bead, 1.05g/cm^3 density, 1 mm diameter, bioreactor rotation of 10 rpm in distilled water at 23°C. In the rotating frame, the particle assumes a primary circular trajectory in a clockwise direction that slowly drifts to the outer wall. In the laboratory frame of reference, the bioreactor is rotating in a counter-clockwise direction.

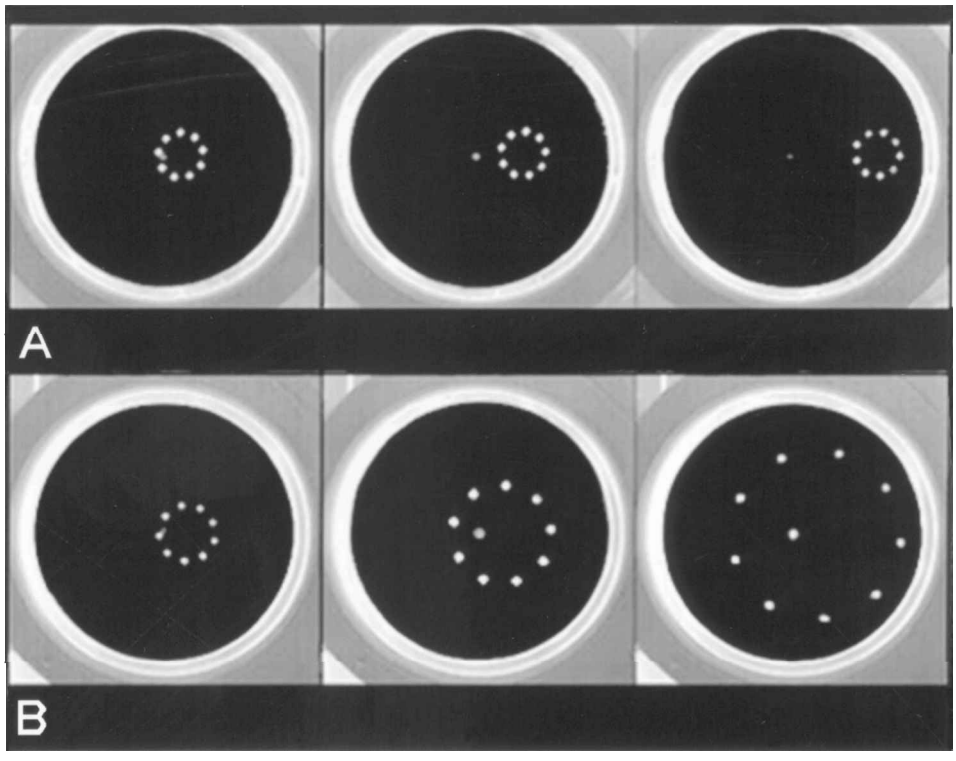

FIG. 4. Bead motion in two observation frames using the imaging tracking system. Polystyrene bead, 1.05 g/cm^3 density, 1 mm in diameter rotating at 18 rpm in distilled water 23°C. Similar results were obtained in culture media at 37°C. In the rotating frame, the camera rotates at the same angular velocity as the bioreactor, in a counter-clockwise direction. In the stationary frame, the camera is stationary in the laboratory frame. (**A**) In the rotating frame, the bead maintains a circle of rotation in the clockwise direction of a constant diameter with its center moving toward the outer wall. (**B**) In the stationary frame, the bead appears to have an increasing circle of rotation in the counter-clockwise direction with a stationary center. The center point of the bioreactor appears as a fixed point in both (**A**) and (**B**).

work we used a non-Stokes flow approximation to obtain numerical solutions giving more precise trajectories that apply to larger-diameter carriers as well as large clusters of microcarrier–cell–tissue constructs.

ANALYTICAL METHOD

We have analyzed the motion of a spherical microcarrier bead inserted into a rotating bioreactor diagrammed in Fig. 1. Upon initiation of bioreactor rotation, the culture medium rapidly achieves steady state (rigid body) motion with respect to the walls of the reactors. Finite element simulations using FIDAP, a commercially available computational fluid dynamics code (Fluent, Inc.), confirmed this, demonstrating that rigid body motion is obtained for typical operating conditions in less than 2 min. However, the microcarriers and cells do not achieve rigid body motion relative to the culture medium when their density differs from that of the medium. Microcarrier motion relative to the rotating fluid is governed by equations of motion, derived in the rotating frame, for the particle position (x, y) and velocity ($v_x v_y$) as follows.[6]

$$\frac{dx}{dt} = v_x,$$

$$\frac{dv_x}{dt} = \frac{1}{\rho_{sphere} \cdot V_{sphere}} \times \begin{bmatrix} p \cdot S \cdot C_d \cdot \dfrac{v_x}{v} + (\rho_{sphere} - \rho_{fluid}) \cdot V_{sphere} \cdot \omega^2 \cdot x \\ +2 \cdot (\rho_{sphere} - \rho_{fluid}) \cdot V_{sphere} \cdot \omega \cdot v_y - (\rho_{sphere} - \rho_{fluid}) \cdot V_{sphere} \cdot g \cdot \sin(\omega t) \end{bmatrix} \quad \frac{dy}{dt} = v_y,$$

$$\frac{dv_y}{dt} = -\frac{1}{\rho_{sphere} \cdot V_{sphere}} \times \begin{bmatrix} p \cdot S \cdot C_d \cdot \dfrac{v_y}{v} + (\rho_{sphere} - \rho_{fluid}) \cdot V_{sphere} \cdot \omega^2 \cdot xy \\ -2 \cdot (\rho_{sphere} - \rho_{fluid}) \cdot V_{sphere} \cdot \omega \cdot v_x - (\rho_{sphere} - \rho_{fluid}) \cdot V_{sphere} \cdot g \cdot \cos(\omega t) \end{bmatrix},$$

$$S = \pi \cdot R_{sphere}^2,$$

$$C_d \approx \frac{24}{\mathrm{Re}} + \frac{6.0}{1/0 + \sqrt{\mathrm{Re}}} + .4$$

where $(\rho_{sphere} - \rho_{fluid})$ is the difference between the density of the microcarrier and surrounding fluid, Re is the Reynolds number, V_{sphere} is the microcarrier volume C_d is the drag coefficient, p is the stagnation pressure, ω is the rotation speed of the bioreactor, S is the microcarrier planar surface area, and Z is the axis of rotation. These equations of motion are solved numerically by employing a fourth-order Runga Kutta integration scheme on a local workstation, using an adaptive stepwise control algorithm (normalized error = 1×10^{-6}) to ensure proper convergence through the integration period, and assuming that the particles initially start at a specific position (x,y) in the bioreactor.

Because we focused on determining the trajectory of the microcarrier and the time it remained suspended in the bioreactor *before* hitting the outer wall, most simulations started with particles at the center of the HARV. Solutions could be terminated when the particle 'stuck' the outer wall of the vessel. The computed time required for the microcarrier to migrate from the center to the outer wall was defined as the residence time for the microcarrier. It should also be noted that for symmetric microcarriers all forces are in the x,y plane so that motion is planar, thus a carrier remains in its plane in this model. Experimental measurements of microcarrier motion confirm this model assumption.

EXPERIMENTAL METHODS

To validate the numerical solutions and to visualize the detailed microcarrier-cell motion relative to the culture medium, we designed and built a particle imaging and tracking apparatus shown in Fig. 2. A CCD camera (Cohu, Inc., San Diego, CA) was mounted on a rotating frame that rotated about the same z-axis of rotation as the bioreactor. The position of the camera within the frame was adjustable along the radius of the rotating frame, thereby allowing the user to scan particles along the diameter of the bioreactor. The bioreactor vessel opposing the rotating camera frame was constructed using the same interior dimensions of a HARV chamber, but the Lucite material in the front of the HARV chamber was replaced by optically transparent Pyrex. The base, or rear face, was painted black to improve contrast with reflected light from beads in the chamber. Both the bioreactor chamber and the camera were driven by separately controlled indexer (stepper) motors (Parker Inc., Rohnert Park, CA) coupled to a custom built gear drive assembly to match precisely their rotation velocities. In addition, a three dimensional micrometer stage is used to align precisely the chamber and the camera. Using appropriate lenses and zoom (0.7× to 4.5×) attachments for the camera, microcarrier trajectories were recorded and individual cells were observed on the microcarrier beads using a low noise slip ring (Mercotac, Carlsbad, CA) for the

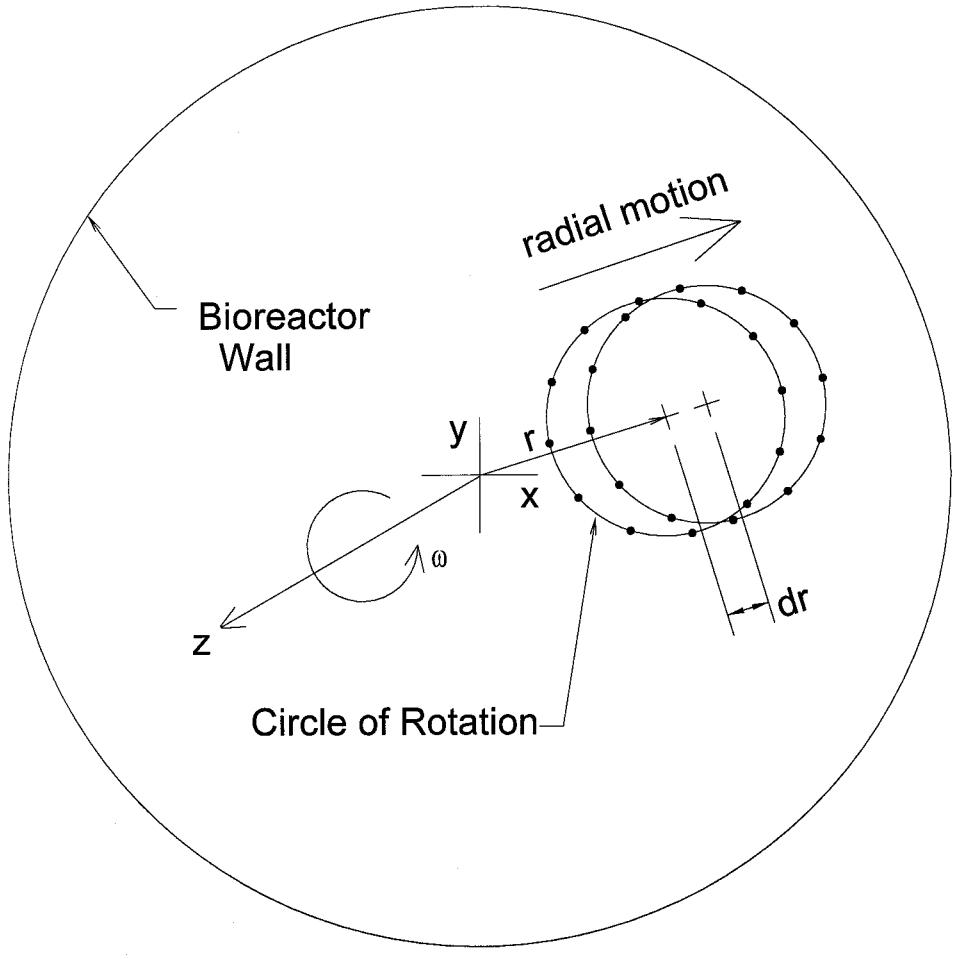

FIG. 5. Measuring radial velocity. r is defined as the radial position from the center of the reactor to the center of the circle of rotation as seen in the rotating frame of reference. dr/dt is the velocity of the radial position of the center of the circle of rotation as seen in the rotating frame.

analog video signal. To eliminate vibration artifact, both the rotating camera frame and rotating bioreactor were mounted on a 10-foot optical workbench (TMS, Inc).

Polystyrene microcarriers of varying density and radius (Solo Hill Engineering, Ann Arbor, MI) were inserted into the reactor; the rotation of the reactor and the camera were started, and microcarrier motions videotaped (Sony VCR SVO-9500 MD, Japan). Prior to the start of each rotation, care was taken to remove all air bubbles. After completion of each experiment, the tapes were re-recorded using a Sony Frame Code Generator for frame-by-frame image post processing using a frame digitizer and frame grabber (Media Cybernetics, Silver Spring MD). An image analysis software package (Image Pro, Phase 3 Imaging, Inc., Glen Mills, PA) installed on a computer system (Gateway, Inc., N. Sioux City, SD) was used to select video frames at regular intervals, subtract unnecessary background signal in each image, and select a microcarrier or a cluster of microcarriers within the field of view over consecutive frames. From the automated particle selection process, a temporal description of the horizontal and vertical bead position was measured from which particle velocities were computed. To determine the outward radial speed of the microcarrier, time-lapse images were taken at fixed intervals until the microcarrier reached the reactor wall and, in some cases, after the collision occurred. The centroid from each image was used to determine the average radial position as a function of time. A time-lapse image of a typical trajectory is shown in Fig. 3. From these data, the position of the centroid, the residence time, and the radial speed was determined at different reactor rotation speeds.

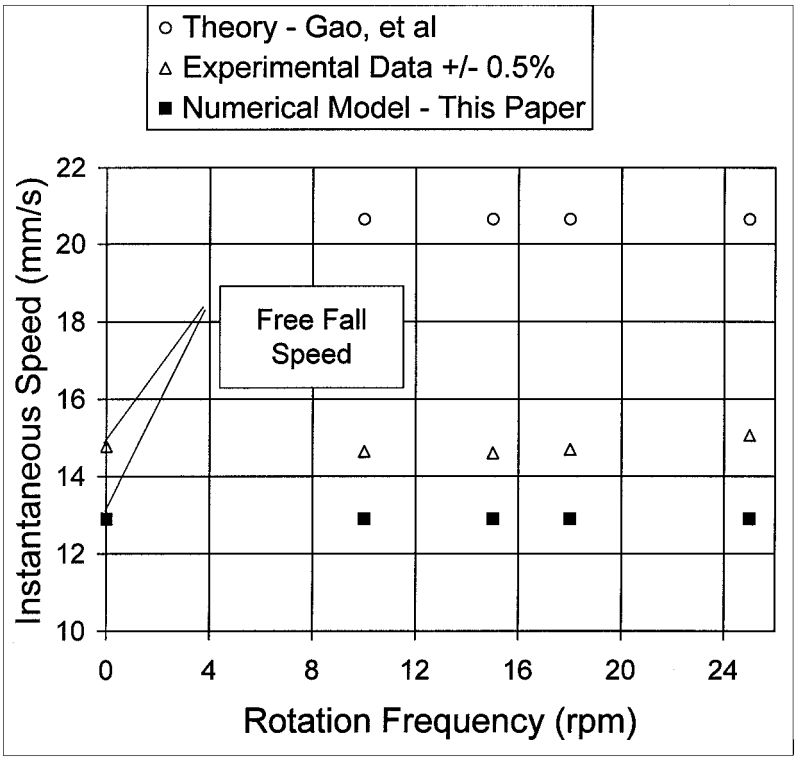

FIG. 6. Influence of rotation frequency on instantaneous speed of a microcarrier in the bioreactor. Polystyrene bead, 1.05 gm/cm^3 density, 1 mm diameter in distilled water at 23°C. Comparison of experimental results including free fall speed to the analytical theory proposed by Gao *et al.* and to our numerical theory using a non-Stokes drag.

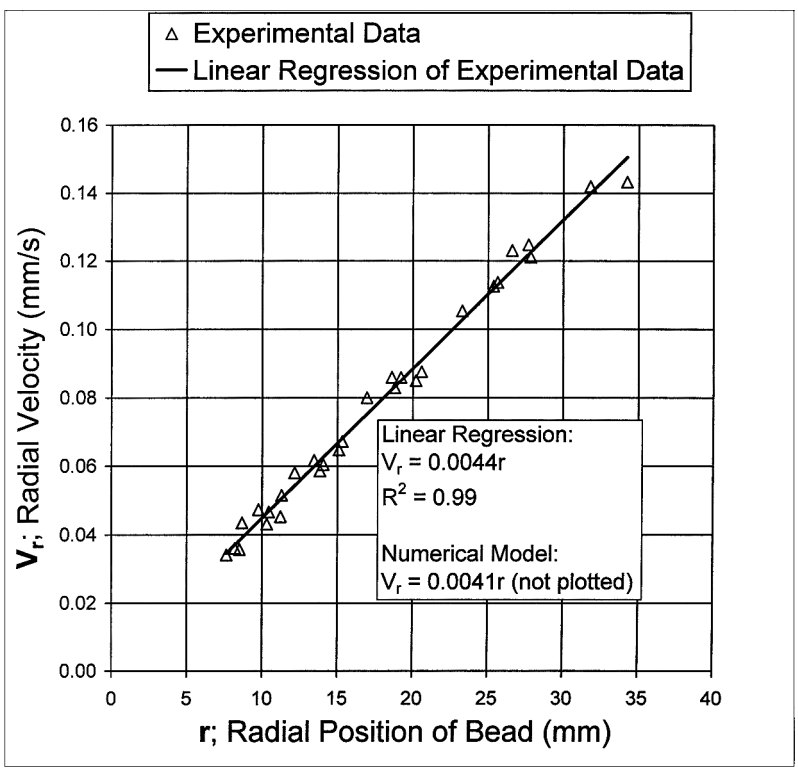

FIG. 7. Comparison of measured and predicted particle radial velocity at 18 rpm for polystyrene bead, (1.05 g/cm^3 density, 1 mm diameter in distilled water at 23°C). A regression of the measured data (solid line) is in excellent agreement with theory as indicated in legend.

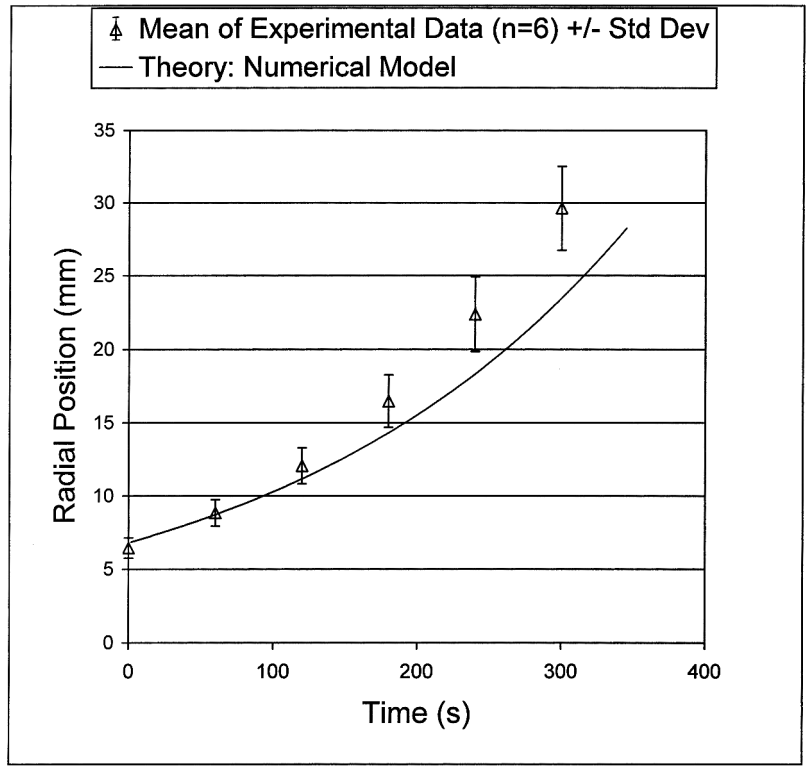

FIG. 8. Comparison of predicted and measured radial particle position (18 rpm, polystyrene bead, 1.05 g/cm^3 density, 1 mm diameter at 18 rpm in distilled water at 23°C). The numerical model closely follows the trend observed from the experimental data.

RESULTS

Three categories of results were obtained: (1) the calculated results of microcarrier trajectories under a variety of experimental simulations; (2) the validation results obtained from image analysis of experimental microcarrier and cluster trajectories; and (3) the observation of lighter-than-water microcarrier self-assembled scaffolds.

For microcarriers with density greater than the culture medium fluid, our results showed that the microcarrier path can be described as two motions in the rotating frame: (1) a periodic circular motion that followed the sedimentation speed of the microcarrier, and (2) an outward radial motion that reflected the centrifugal drift on the microcarriers in the rotating frame (see Fig. 3, 4 and 5). The instantaneous microcarrier velocity in the rotating frame was determined directly from microcarrier position data by dividing the distance traveled along the circle of rotation during the sampling period by the elapsed time. No statistically significant variation in the instantaneous microcarrier speed occurred with a change in the rotation speed of the bioreactor. These values were compared to the measured free fall speed of the same microcarriers as shown in Fig. 6. Moreover, measured microcarrier speeds for all bioreactor rotation speeds were consistently less than those predicted in a previous analytical model by Gao *et al*,[5] and are slightly above but much closer to the speeds predicted by this numerical model (Fig. 6).

Detailed measurements of radial velocity versus radial position are shown in Fig. 7. In this figure, radial velocity is defined as the velocity of the center of circular motion as viewed in the rotating frame and the radial position is the position of the center of circular motion as viewed in the rotating frame, as described in Fig. 5. Excellent agreement with theory is noted. Over time, the radial position of the microcarrier increased for a given set of bioreactor operating conditions when the density of the microcarrier was greater than the density of the media. The measured temporal change in radial position from four in-

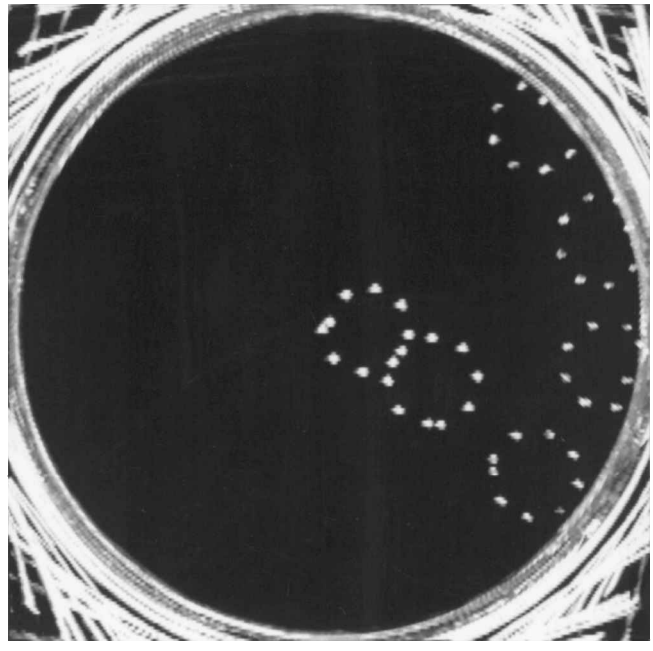

FIG. 9. Bead tracking results showing the temporal evolution of particle trajectory. Polystyrene bead, (1.05 g/cm^3 density, 1 mm diameter in distilled water at 23°C) was tracked serially as the particle moved from the center to the wall of the bioreactor. Once the bead reached the wall, interaction between the bead and the wall produced a frictional force that caused a tangential movement of the circle of rotation resulting in repeated collisions with the bioreactor wall. The bioreactor was rotating in the counter-clockwise direction in the laboratory frame of reference.

dependent sets of measurements was in excellent agreement with the predicted results of the numerical model as seen in Fig. 8. Images from the tracking system showed that the radial position of the particles slowly moved to the outer wall until the particle began interacting or striking the wall of the bioreactor (Fig. 9). Once the particle collided with the outer wall of the bioreactor, the circular orbits changed to reflect the particle rolling along the bioreactor wall for a portion of the revolution. From the frictional interactions present during this rolling phase, the particle moved circumferentially along the outer wall of the bioreactor as seen in Fig. 9. Unless the bioreactor was stopped, this partial rolling of the particle along the outer wall continued.

"Residence time," defined as the time the particle was suspended in the fluid before hitting the wall, was affected by physical parameters of the microcarriers and the fluid medium as shown in Fig. 10. For example, residence time was nonlinearly related to the density above that of the medium rapidly decreased the residence time. Increasing fluid viscosity linearly increased the predicted residence time (Fig. 10b), whereas raising the rotational speed significantly reduced residence time (Fig. 10c).

When the microcarrier density was less than that of the culture medium, the centrifugal force reversed and the microcarriers migrated toward the center of the reactor. This novel and important observation is depicted in Fig. 11 for polystyrene beads of relative density 0.98 and mean diameter of 160 μm. The clustering near zero radius is evident.

DISCUSSION

We have applied the equations of motion to develop a numerical solution to the trajectory of a microcarrier, using a non-Stokes drag force component, in a high aspect ratio rotating bioreactor. The results, while similar to those of Gao[5] for heavier-than-water microcarriers, are more accurate in cases of larger microcarriers and aggre-

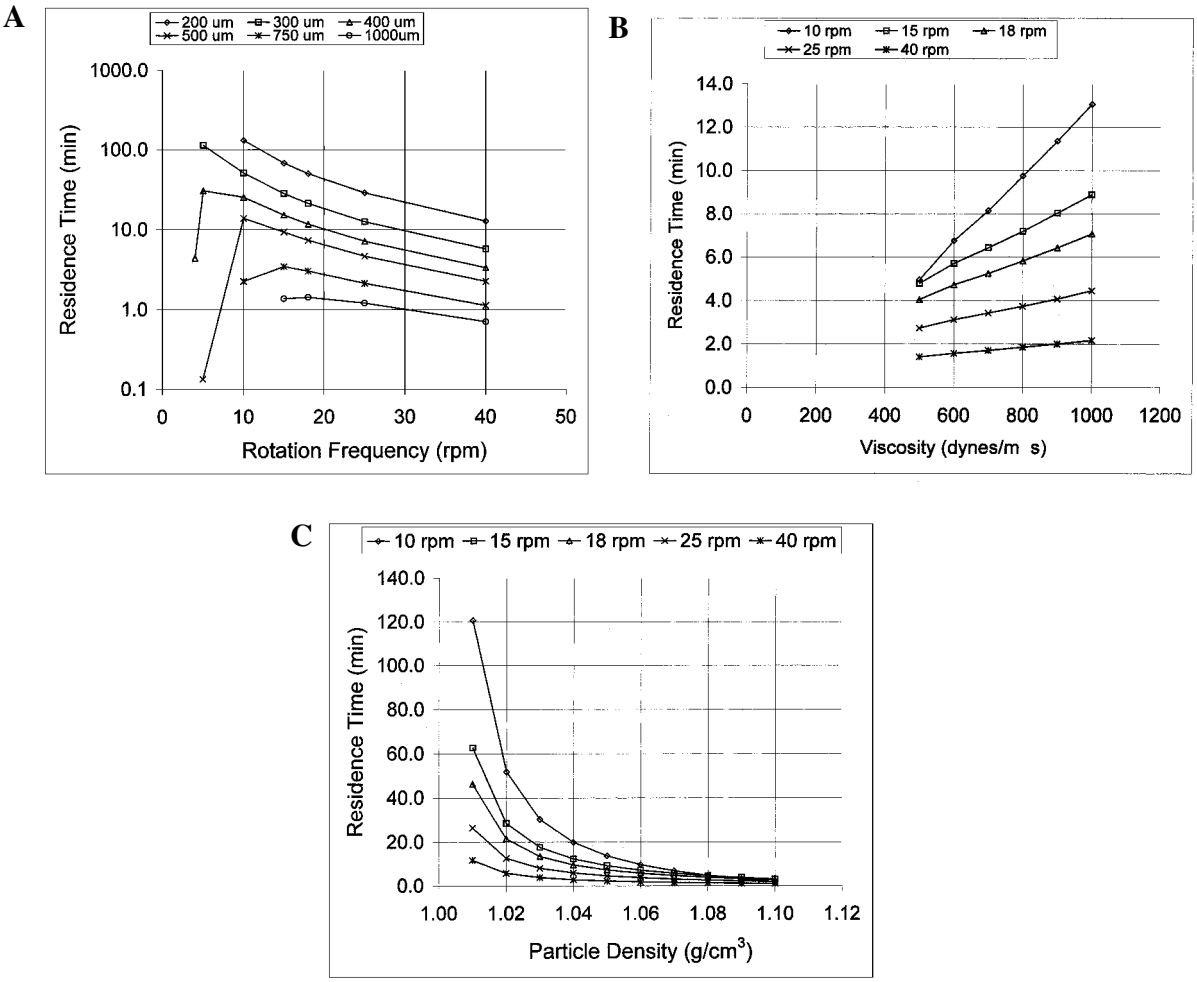

FIG. 10. Parametric analysis of particle trajectory from numerical model. Particle size significantly influences residence time of a particle in the bioreactor (**A**), media viscosity linearly changes the residence time of a particle in the bioreactor (**B**), particle specific gravity (media s.g. = 1.0) strongly affects the residence time of particles in the bioreactor (**C**).

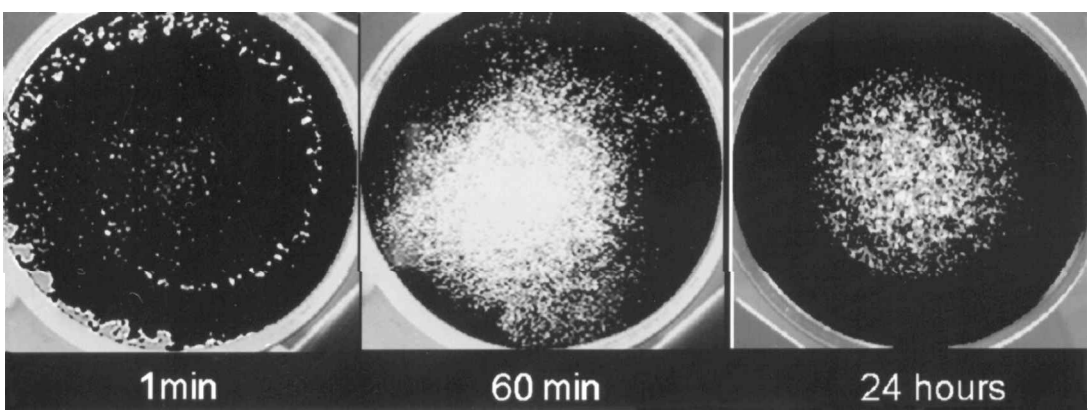

FIG. 11. Microcarrier bead tracking results using lighter than medium ($\rho_{bead} < \rho_{medium}$) Polystyrene beads, (0.98 g/cm^3 density, ~160 um diameter at 18 rpm in cell culture medium at 37°C). One minute after initiation of rotation, momentum transfer from the chamber walls to medium has produced an inward spiral pattern of the beads. After 60 min, the beads have nearly reached their steady state position, which is shown at 24 h.

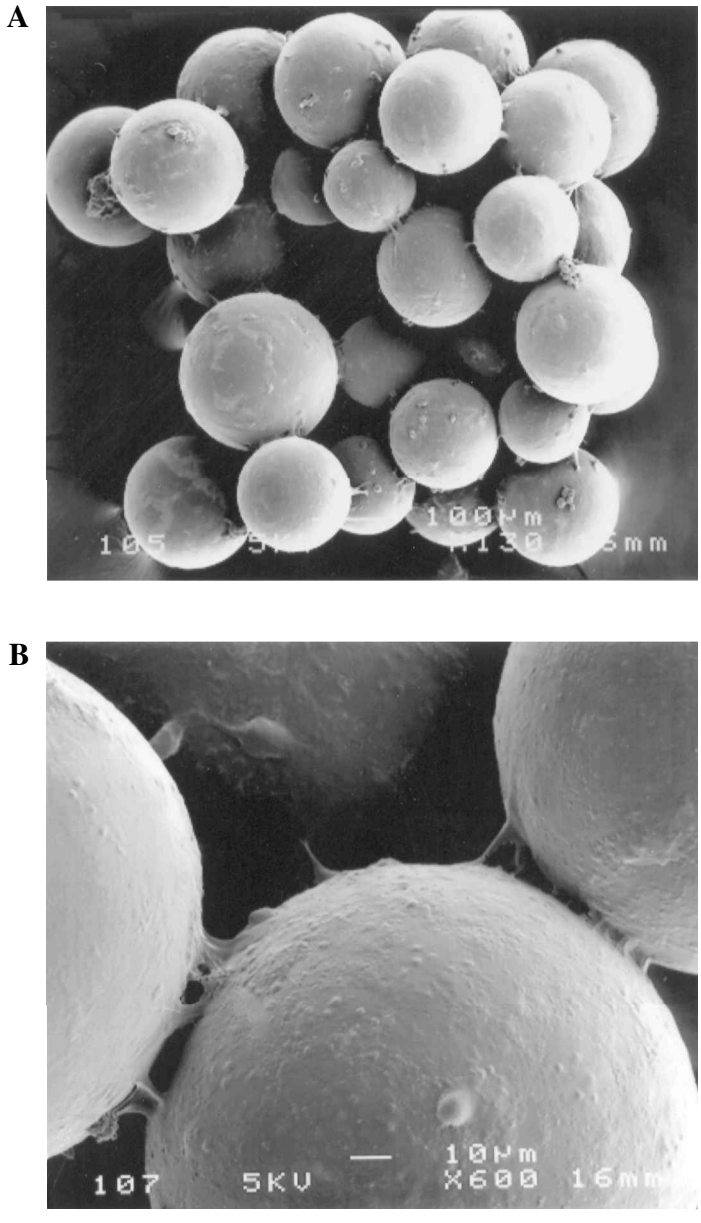

FIG. 12. SEM photographs of lighter-than-water microcarriers (density = 0.98 gms/cc density) after 24 h (**A**), and at higher magnification (**B**), in the bioreactor at 18 rpm seeded with Saos-2 human osteoblasts. Tissue bridges after 24 h in the bioreactor are evident in both (**A**) and (**B**).

gates. Our analysis predicted that lighter-than-water microcarriers should aggregate and self-assemble in the central region of the rotating vessel. These predictions have been validated with an imaging system that was used to determine trajectories of microcarriers whose densities were both greater and less than that of water. Our imaging system has also been used by Qing-Qing *et al.*[7] to obtain their results with hollow bioceramic microspheres.

It was clearly confirmed in our work that heavier than medium microcarriers make repeated collisions with the wall of the rotating vessel. Although cell damage in dynamic bioreactors has been discussed[8] with regard to effects of this confounding variable on tissue engineering, the effects in the rotating high aspect ratio vehicle used here have not been studied. One significant advantage of the lighter-than-water microcarriers in this bioreactor is that this unquantified mechanical "stimulus" is avoided by the microcarrier in the

central region of the bioreactor. Another advantage of the lighter-than-water microcarriers is that the central region of the rotating bioreactor is accessible to optical technologies, allowing the study of reactor-particle kinematics as well as the use of selected dyes for more extensive real-time nondestructive analysis of biophysical and biochemical cellular mechanisms. This is currently under development in our laboratories.

Finally, the secondary circular motion of the lighter-than-water microcarrier scaffolds around the central axis of the reactor provides a convective transport flux for the mixing of the culture medium and flow of nutrients within the porous scaffold. The effects of this transport of nutrients to the interior regions of the scaffolds may permit bone growth (Fig. 12) that is enhanced by both nutrient flow[9,10] and the three-dimensional configuration of the scaffold. This issue is also being explored in studies we have undertaken on bone tissue engineering.

ACKNOWLEDGMENT

We thank NASA for funds to perform this work with research grant NAG9-832.

REFERENCES

1. Prewett, T.L., Goodwin, T.J. and Spaulding, G.F., Three dimensional modeling of T.24 human bladder carcinoma cell line: A new simulated microgravity vessel. J. Tissue Culture Meth. **15,** 29, 1993.
2. Goodwin T.J., Prewett, T.L., Spaulding, G.F., and Becker, J.L. Three-dimensional culture of a mixed mullerian tumor of the ovary: Expression of in vivo characteristics. In Vitro Cell. Develop. Biol. Animal **33,** 366, 1997.
3. Freed, L.E., and Vunjak-Novakovic, G. Microgravity tissue engineering. In Vitro Cell. Develop. Biol. Animal **33,** 381, 1997.
4. Wolf, D.A., and Schwarz, R.P. Experimental measurement of the orbital paths of particles sedimenting within a rotating viscous fluid as influenced by gravity. NASA Technical Paper 3200, 1992.
5. Gao, H., Ayyaswamy, P.S., and Ducheyne, P. Dynamics of a microcarrier particle in the simulated microgravity environment of a rotating-wall vessel. Microgravity Sci. Technol. X/3, 154, 1997.
6. Meaney, D., Johnston, E., Litt, M., and Pollack, S. Experimental and numerical investigations of microcarrier motions in simulated microgravity. Adv. Heat Mass Transfer Biotechnol. HTD-vol. **362,** 103, 1998.
7. Qing-Qing, Q., Ducheyne, P., and Ayyaswamy, P.S. Fabrication, characterization and evaluation of bioceramic hollow microspheres used as microcarriers for 3-D bone tissue formation in rotating bioreactors. Biomaterials **20,** 989, 1999.
8. Cherry, R.S., and Papoutsakis, E.T., Physical-mechanisms of cell-damage in microcarrier cell-cultures bioreactors. Biotechnol. Bioeng. **32,** 1001, 1998.
9. Allen, F.D., Hung, C.T., Pollack, S.R., and Brighton, C.T. Evidence for mechano-chemical coupling in the activation of flow-induced [Ca2+]; response in rat primary cultured bone cells. J. Biomech. (submitted), 2000.
10. Jacobs, C., Yellowley, D.A., Harper, R.A., and Katz, J.L. Differential effect of steady versus oscillating flow on bone cells. J. Biomech. **31,** 969, 1998.
11. Hung, C.T., Pollack, S.R., Reilly, T.M., and Brighton, C.T. Comparison of the [Ca^{2+}] response to fluid flow of MC3T3-E1, ROS 17/2.8 and cultured primary osteoblast-like cells. Cell. Eng. **1,** 117, 1996.

Address reprint requests to:
S.R. Pollack, Ph.D.
Professor
Department of Bioengineering
University of Pennsylvania
Philadelphia, PA 19104

E-mail: be@spollack@seas.upenn.edu